Supporting Information for

Designing electrolytes with high solubility of sulfides/disulfides for high-energy-density and low-cost K-Na/S batteries

Liying Tian[1,2], Zhenghao Yang[1], Shiyi Yuan[1], Tye Milazzo[3], Qian Cheng[1], Syed Rasool[1], Wenrui Lei[4], Wenbo Li[1], Yucheng Yang[1], Tianwei Jin[1], Shengyu Cong[1], Joseph Francis Wild[1], Yonghua Du[5], Tengfei Luo[*4], Donghui Long*[2], Yuan Yang*[1]

1. Department of Applied Physics and Applied Mathematics, Columbia University, New York, NY 10027, United States

2. Key Laboratory of Chemical Engineering, East China University of Science and Technology, Shanghai, 200237, China.

3. Department of Aerospace and Mechanical Engineering, University of Notre Dame, Notre Dame, IN 46556, United States

4. Department of chemistry, Columbia University, New York, NY 10027, United States

5. National Synchrotron Light Source II, Brookhaven National Laboratory, Upton, NY 11973, United States

These authors contributed equally: Liying Tian, Zhenghao Yang

***Corresponding author:**

E-mail: yy2664@columbia.edu (Yuan Yang), longdh@mail.ecust.edu.cn (Donghui Long), tluo@nd.edu (Tengfei Luo)

Table of Content

Supplementary Notes 3
Supplementary Note 1. Reported works on Na/S and K/S batteries 3
Supplementary Note 2. Calculation of specific energy 5
Supplementary Note 3. Molecular dynamic simulations 7
Supplementary Note 4. The effect of carbon powder to improve wettability of BASE/anode 12
Supplementary Note 5. Diffusion Coefficient Calculation 13
Supplementary Note 6. The discussion about better cycling stability of K-Na/S cells with TEGDME catholyte 14
Supplementary Note 7. Material Cost estimation of K-Na/S battery system 15
Supplementary Figures 16

Supplementary Notes

Supplementary Note 1. Reported works on Na/S and K/S batteries

Supplementary Table 1.

Reported works on RT Na/S and K/S batteries

Na/S battery	Design strategy	Current (mA cm^{-2} / mA g^{-1})	Average voltage (V)	Initial capacity (mAh/g)	Cycle number	Normalized decay (%/100 cycles)
[1]	SPAN	NA / 267	1.32	1510	100	6.5
[2]	Mo_2N–W_2N@PC	0.90 /1000	1.30	860	400	12.0
[3]	FeS_2@ NCMS/S	NA /100	1.25	770	300	12.0
[4]	Small sulfur molecules	1.68 / 1675	1.20	700	2000	0.3
[5]	3D-PNCV	NA / 5000	1.38	561	800	2.9
[6]	Co@PCNFs/S	1.64 / 830	1.45	530	600	4.6
[7]	S/MoS_2/NCS	NA / 1000	1.40	427	2800	0.6
K/S battery	**Design strategy**	**Current (mA/cm^2 / mA/g)**	**Average voltage (V)**	**Initial capacity (mAh/g)**	**Cycle number**	**Normalized decay (%/100 cycles)**
[8]	Small sulfur molecules	0.02 / 20	1.00*	1198	150	19.3
[9]	S–N–Cos–C	NA / 200	1.25*	463	150	16.2
[10]	Homogeneous catalyst	NA/800	1.93	650	200	8.4
[11]	Concentrated electrolyte	NA/10	2.10	606	NA	NA
This work	**Amide electrolyte**	**2 / 600**	**2.10**	**830**	**1100**	**3.2**

Supplementary Table 2.

Reported works on Intermediate Temperature (IT) Na/S and K/S batteries

Na/S battery	**Design strategy**	**Current (mA/cm^2)**	**Average voltage (V)**	**Initial capacity (mAh/g)**	**Cycle number**	**Normalized decay (%/100 cycles)**	**Operation temperature (°C)**
[12]	TEGDME catholyte	2.33	1.80	428	60	44.8	150
[13]	Na-Cs alloy	2.33	1.88	420	100	3.0	95
[14]	LAT heat-treating	4.67	1.92	339	1000	<0.1	120
K/S battery	**Design strategy**	**Current (mA/cm^2)**	**Average voltage (V)**	**Initial capacity (mAh/g)**	**Cycle number**	**Normalized decay (%/100 cycles)**	**Operation temperature (°C)**
[15]	TEGDME catholyte	1.33	2.00	312	1000	<0.1	150
This work	**Dissolving K_2S and K_2S_2**	**2.00**	**2.10**	**830**	**1100**	**3.2**	**75**

*In these two references, the average voltage in RT K/S is 1.0 and 1.2 V, respectively, which is much lower than IT K/S batteries (2.1 V in our report and 2.0 in reference 15). This arises from that they use small molecule sulfur, where sulfur exists as S_x (S = 1-4), which is known to have a lower voltage than S_8, the common form of S cathode (e.g., ~1.7 V vs. 2.1 V), in Li-S batteries[16,17]. When S_8 is used, the voltage of RT K/S batteries is also around 2.0 V, as shown in references 10 and 11, which is similar to our IT K/S batteries.

Supplementary Note 2. Calculation of specific energy

The theoretical specific energy is calculated based on the stoichiometric ratio of sulfur and K, and the theoretical capacity of sulfur (1675 mAh g^{-1}) and K (687 mAh g^{-1}). Only the mass of sulfur, K, and CPL/acetamides are considered. Therefore, as shown in Table S3 below, for 1 Ah cell, the mass of sulfur and K are 0.597 g and 1.46 g, respectively (Supplementary Table 3). The mass of CPL/acetamide depends on [S], and it is calculated to be 18.6 g, 4.66 g, and 2.33 g for 1 M, 4 M and 8 M, respectively. Hence the total mass for 1 Ah cell is 20.7 g, 6.71 g, and 4.38 g, respectively. Given that the average voltage of K-Na/S cells is 1.98 V, the theoretical specific energy of K-Na/S batteries is 95.8, 295, and 452 Wh/kg for 1, 4, and 8 M [S]. The specific energy of other concentrations is calculated with the same procedure.

Supplementary Table 3.

Calculation of theoretical energy density for K-Na/S cells

[S] (M)	Capacity (Ah)	Average voltage (V)	Sulfur mass (g)	Potassium mass (g)	CPL/acetamide (g)	Total mass (g)	Specific energy (Wh/kg)
1	1.00	1.98	0.597	1.46	18.6	20.7	95.8
4	1.00	1.98	0.597	1.46	4.66	6.71	295
8	1.00	1.98	0.597	1.46	2.33	4.38	452

The calculation of practical specific energy at the cell level is shown in Supplementary Table 4, we use the practical capacity of electrodes (e.g., 1000 mAh g^{-1} sulfur and 600 mAh g^{-1} for K). Moreover, the masses of BASE and packaging are taken into account.

For BASE, we assume that its thickness is 0.5 mm and its density is 3.31 g cm^{-3} [18] so its mass is 1.66 kg m^{-2}. The electrode mass per area depends on the current density and discharge time. Take 2 mA cm^{-2} and 24-hour discharge as an example, the areal capacity is 48 mAh cm^{-2}, so the mass of sulfur is 48 mAh cm^{-2} / 1000 mAh g^{-1} = 0.48 kg m^{-2}. Similarly, the mass of K is 0.80 kg m^{-2}. The mass of CPL/acetamide is 15, 3.75, and 1.88 kg m^{-2} for 1 M, 4 M, and 8 M [S] respectively. For packaging, we assume that the packaging is Al with a thickness of 0.05 mm, so the mass of Al on the two sides together is 0.27 kg m^{-2}.

Take a footprint area of 100 cm^2, 4 M sulfur and a discharge time of 24 hours as an example, the total energy is 48 mAh cm^{-2} × 1.98 V × 100 cm^2 = 9.50 Wh. The total mass is 4.80 g + 8.00 g + 37.5 g + 16.6 g + 2.7 g = 69.6 g, and thus the specific energy is 136 Wh kg^{-1}.

When the discharge time increases to one week, the mass of each component above can be calculated similarly, and we summarize the data in Supplementary Table 5 below.

Supplementary Table 4.

Calculation of practical energy density for 24-hour discharge at 2 mA cm^{-2} and 100 cm^2 area

[S] (M)	Capacity (Ah)	Average voltage (V)	Sulfur mass (g)	Potassium mass (g)	CPL/acetamide mass (g)	BASE mass (g)	Packaging mass (g)	Total mass (g)	Specific energy (Wh/kg)
1	4.80	1.98	4.80	8.00	150	16.6	2.70	182	52.1
4	4.80	1.98	4.80	8.00	37.5	16.6	2.70	69.6	136
8	4.80	1.98	4.80	8.00	18.8	16.6	2.70	50.9	186

Supplementary Table 5.

Calculation of practical energy density for one-week discharge at 2 mA cm^{-2} and 100 cm^2 area

[S] (M)	Capacity (Ah)	Average voltage (V)	Sulfur mass (g)	Potassium mass (g)	CPL/acetamide mass (g)	BASE mass (g)	Packaging mass (g)	Total mass (g)	Specific energy (Wh/kg)
1	33.6	1.98	33.6	8.00	1050	16.6	2.70	1111	57.3
4	33.6	1.98	33.6	8.00	263	16.6	2.70	323	179
8	33.6	1.98	33.6	8.00	132	16.6	2.70	192	276

Supplementary Note 3. Molecular dynamic simulations

To complement the experimental study, we used Molecular dynamic (MD) simulations to calculate the solvation free energy of different solutes (e.g., K_2S and K_2S_2) and solvents (e.g., CPL/acetamide and TEGDME) and to examine the radial distribution function (RDF) for key atoms. We first recreate the molecular structures in Avogadro and assign the Generalized Amber Force Field (GAFF) parameters for each molecule using the Maginn Force Field Archive (MAFFA).[19] It also assigns atomic partial charges using the Restrained ElectroStatic Potential (RESP) method[19]. Parameters used for the simulation are listed in Supplementary Table S3-S9 below, and 3D visualizations of solvent molecules are shown in Supplementary Fig. 3. The simulations use the Verlet neighbor searching scheme with a coulomb cut-off distance of 1.2 nm. The short-range force cutoff is set to 1.0 nm for van der Waals (vdW) interactions. The long-range electrostatic interactions are calculated using the Fast smooth Particle-Mesh Ewald (SPME)[20] method. We then create a 7.1 nm by 7.1 nm by 7.1 nm box and fill it with 600 molecules of solvent, then 1 molecule of the solute. The MD simulations are then performed using the Groningen Machine for Chemical Simulations (GROMACS) package.[21]

We begin our simulations with minimization and equilibration steps for each solvent-solute combination. The minimization is performed using the steepest decent algorithm for energy. For the equilibration steps, the simulation run in the constant pressure, constant temperature (NPT) ensemble. The pressure control uses the exponential relaxation pressure coupling with a time constant of 2 ps and a target pressure of 1 bar. After equilibration, production runs are then performed in the NPT ensemble to calculate the Gibbs free energy.

The free energy is calculated using both the Multistate Bennett Acceptance Ratio (MBAR) and the thermodynamic integration (TI) methods.[22,23] An interaction coupling factor, λ, is then introduced into the non-bonding interaction between the solute and solvent molecules. This controls the states of interaction, starting with a completely un-interacting system ($\lambda = 0$) and gradually forming a fully interacting environment ($\lambda = 1$). The 24 discrete λ, each corresponding to an MD simulation, are sampled and a Python code (alchemlyb)[22] collects results from each simulation and calculates the solvation free energy using MBAR and TI through alchemical analysis. Furthermore, we use the fully interacting system to calculate RDF from atom pairs of interest.

Supplementary Table 6. Parameters for force field generation

Parameter	Value/Status
Periodic boundary conditions	All direction (xyz)
Coulomb type	PME
Coulomb cut-off	1.0 nm
Relative dielectric constant	Infinity
short-range neighbor list cut-off	1.0 nm
Switch to the Lennard-Jones Potential	0.8 nm
Lennard-Jones Potential cut-off	1.0 nm
PME interpolation order	6
Dipole correction to the Ewald summation	off
Constraints	h-bonds
Neighbor searching type	grid

Supplementary Table 7. Simulated atomic properties

Element	Atom name	Atomic number	Mass	Sigma	Epsilon
Carbon	c	6	12.01	0.34	0.359825
Carbon	c3	6	12.01	0.34	0.457728
Hydrogen	hc	1	1.008	0.265	0.065693
Nitrogen	n	7	14.01	0.325	0.711277
Hydrogen	h1	1	1.008	0.2471	0.065693
Hydrogen	hn	1	1.008	0.1069	0.065693
Oxygen	o	8	16	0.296	0.878639
Sulfur	s	19	39.098	0.3919	1.9664
Potassium	k	16	32.0065	0.34	0.359825

Supplementary Table 8. Parameters for acetamide

Atom name	Atom label	Charge
c	C1	0.899919
c3	C2	-0.59354
hc	H1	0.158528
hc	H2	0.158528
hc	H3	0.158528
n	N1	-0.99291
hn	H4	0.41125
hn	H5	0.41125
o	O1	-0.61156

Supplementary Table 9. Parameters for CPL

Atom Type	Atom label	Charge	Atom Type	Atom label	Charge
c	C1	0.550443	hc	H6	0.011927
c3	C2	-0.07018	c3	C6	0.027377
c3	C3	0.07708	hc	H7	0.002399
hc	H1	0.032951	hc	H8	0.002399
hc	H2	0.032951	n	N1	-0.4892
c3	C4	-0.07475	h1	H9	0.045544
hc	H3	0.003736	h1	H10	0.045544
hc	H4	0.003736	hn	H11	0.307088
c3	C5	0.06683	o	O1	-0.5878
hc	H5	0.011927			

Supplementary Table 10. Parameters for TEGDME

Atom Type	Atom label	Charge	Atom Type	Atom label	Charge
c3	C1	0.141638	c3	C6	0.450922
os	O1	-0.43162	c3	C7	0.399088
h1	H1	0.020538	h1	H12	-0.0504
h1	H2	0.020538	h1	H13	-0.0504
h1	H3	0.020538	os	O4	-0.65208
c3	C2	0.17605	h1	H14	-0.03519
c3	C3	0.479352	h1	H15	-0.03519
h1	H4	0.008224	c3	C8	0.479352
h1	H5	0.008224	c3	C9	0.17605
os	O2	-0.65208	h1	H16	-0.06056
h1	H6	-0.06056	h1	H17	-0.06056
h1	H7	-0.06056	os	O5	-0.43162
c3	C4	0.399088	h1	H18	0.008224
c3	C5	0.450922	h1	H19	0.008224
h1	H8	-0.03519	c3	C10	0.141638
h1	H9	-0.03519	h1	H20	0.020538
os	O3	-0.69822	h1	H21	0.020538
h1	H10	-0.0504	h1	H22	0.020538
h1	H11	-0.0504			

Supplementary Table 11. Parameters for K_2S_2

Atom Type	Atom label	Charge
S	S1	-0.99999999
S	S2	-0.99999999
K	K1	0.99999999
K	K2	0.99999999

Supplementary Table 12. Parameters for K_2S

Atom Type	Atom label	Charge
S	S1	-1.99999998
K	K1	0.99999999
K	K2	0.99999999

Supplementary Note 4. The effect of carbon powder to improve wettability of BASE/anode

Molten Na metal shows poor wetting on the BASE sheet, being a significant challenge in reducing the operating temperature of high-temperature Na-S batteries[6]. Although K-Na alloy demonstrates improved wetting on the BASE sheet, achieving satisfactory contact with ceramics at lower temperatures (<100°C) remains an issue[24]. As shown in Supplementary Fig. 6a, the K-Na alloy does not wet a BASE sheet, displaying a contact angle larger than 90 degrees at 75 °C.

To solve the above problem, we add a small amount of carbon black (CB) can effectively immobilize K-Na alloy and improve wetting between K-Na and BASE. The K-Na/C mixture exhibits non-Newtonian fluid properties and adheres well to the surface of the current collector.[25] Our studies shows that such K-Na alloy with carbon additives wets BASE very well (Supplementary Fig. 6).

To further investigate the impact of carbon powder additive, symmetric cells with K-Na alloy and K-Na/C alloy were tested at different current densities. While both K-Na and K-Na/C cells exhibited stable cycling, the overpotential and the resistance of K-Na/C cells was half that of K-Na cells (Fig. 3a, Supplementary Fig. 7).

Supplementary Note 5. Diffusion Coefficient Calculation

The diffusion coefficient in cells with TEGDME electrolyte is calculated by the Warburg impedance. Warburg impedance is defined as:

$$Z_w = \frac{\sigma_W}{\omega^{1/2}} - j\frac{\sigma_W}{\omega^{1/2}}$$

In this equation, σ_W represents the Warburg coefficient, which corresponds to the slope of the diffusion tail in the Nyquist plot. w is angular frequency. The Warburg coefficient can be calculated using the following formula:

$$\sigma_W = \frac{RT}{n^2F^2A\sqrt{2}}\left(\frac{1}{D_{M^+}^{1/2}C_{M^+}}\right)$$

In the equations above, C_{M+} represents the concentration of alkali metal ions.

For curves without a diffusion tail, such as those in cells with CPL/acetamide, the diffusion coefficient is estimated from the ionic conductivity, since the redox participants are soluble in the electrolyte. The diffusivity is estimated from the Nernst-Einstein relation.

$$\sigma_i = \frac{c(zF)^2D_i}{RT}$$

In the measurement, we assume that the transference is 0.5. The corresponding impedance results for conductivity is shown as Supplementary Fig 14.

Supplementary Note 6. The discussion about better cycling stability of K-Na/S cells with TEGDME catholyte

The enhanced stability observed in TEGDME compared to acetamide/caprolactam CPL/acetamide cells are considered to arise from the following three main factors:

1. Cycling duration time. TEGDME and acetamide/CPL cells are cycled at an identical current density. However, due to the significantly higher specific capacity of acetamide/CPL cells, the duration of one cycle is approximately 2 to 3 times longer than that of TEGDME. This extended cycling period likely contributes to greater degradation in the acetamide/CPL cells (e.g. aging of coin cell gaskets and PTFE sealing O rings).

2. Vapor pressure. The boiling points of the solvents show notable differences: TEGDME has a high boiling point of 275°C, while acetamide and CPL boil at 220°C and 270°C, respectively. The formation of a eutectic solvent in the mixture could further reduce its boiling point. Correspondingly, the vapor pressure trends align with boiling point data. CPL or acetamide exhibits higher vapor pressure compared to TEGDME. For instance, acetamide alone has a vapor pressure of 10.25 kPa at 100°C[26], whereas TEGDME's vapor pressure is substantially lower at 132 Pa[27] at 100°C. This disparity suggests that evaporation could be more pronounced in CPL/acetamide than in TEGDME.

3. Solubility of K_2S_2. During the discharge process, solid K_2S_2 is formed. However, the majority of the specific capacity is attributed to the soluble S/K_2S_3 redox reaction. Since the transformation mostly happens from S to K_2S_3, a small amount of solid precipitation will not lead to the irreversibility of reaction.

Supplementary Note 7. Material Cost estimation of K-Na/S battery system

In material cost estimation, we take the cost of sulfur, K, CPL/acetamide, BASE and packaging into account, and we use the practical specific capacities for generating the 1-day discharge and 1-week discharge curves in Fig. 1b (see Supplementary Note 2). The cost of these materials per weight is listed in Supplementary Table S13.

Supplementary Table 13.
Reactor Components Cost per Area

Components	Price ($ kg^{-1})
Sulfur	0.2
CPL/acetamide	6.5
K metal	12.1
BASE	10
Aluminum	2.3

Based on these prices, we can calculate the cost of each component in K-Na/S batteries for the same configurations in Fig. 1b. Here we use 1-day discharge as an example, and the results are shown in Supplementary Table 14. Again, we assume the current density is 2 mA cm^{-2} and the footprint area is 1 m^2.

Supplementary Table 14.
Calculation of cost of K-Na/S batteries for 1-day discharge at 2 mA cm^{-2} and 1 m^2 area

[S] (M)	Capacity (Ah)	Average voltage (V)	Sulfur cost ($)	Potassium cost ($)	CPL/acetamide cost ($)	BASE cost ($)	Packaging cost ($)	Total cost ($)	Cost per energy ($/kWh)
1	480	1.98	0.096	9.68	97.5	16.6	0.621	124.5	131
4	480	1.98	0.096	9.68	24.4	16.6	0.621	51.4	54.1
8	480	1.98	0.096	9.68	12.2	16.6	0.621	39.2	41.2

Supplementary Figures

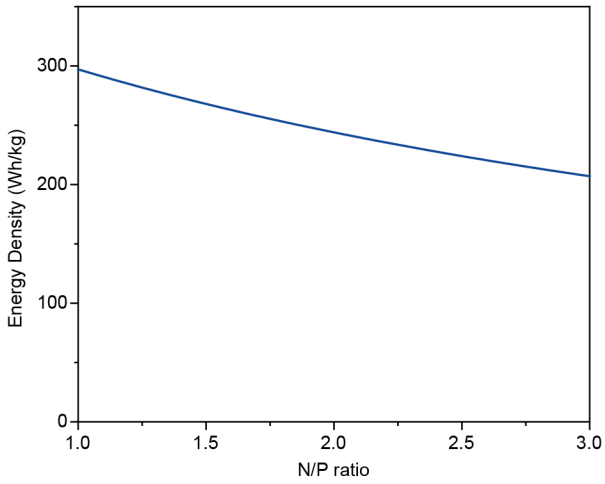

Supplementary Fig. 1. The Negative electrode active material/Positive electrode active material molar ratio dependence of theoretical energy density for K-Na/S battery with 4 M [S]. The mass of solvent and active material is considered in the calculation.

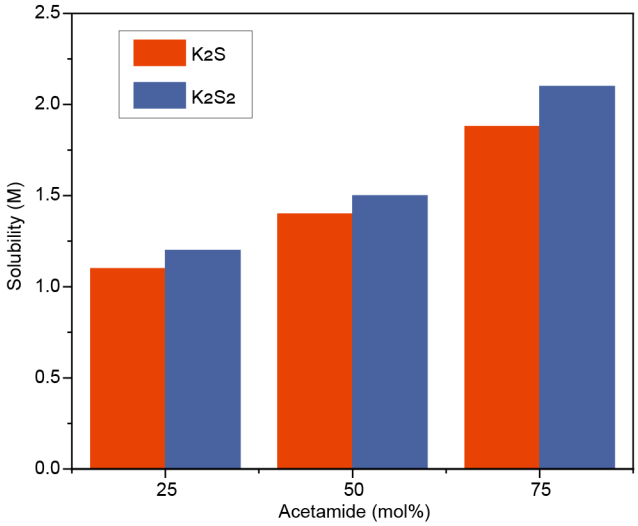

Supplementary Fig. 2. Solubility of K_2S and K_2S_2 for CPL/acetamide mixture with different acetamide fractions.

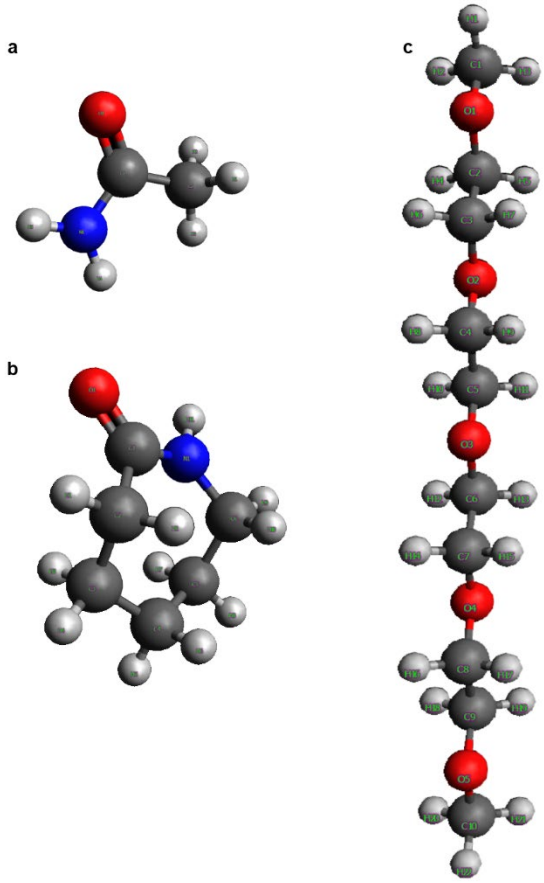

Supplementary Fig. 3. 3D structures for (a) Acetamide, (b) CPL, and (c) TEGDME used in simulation. Blue: N, Red: O, Grey: C, White: H.

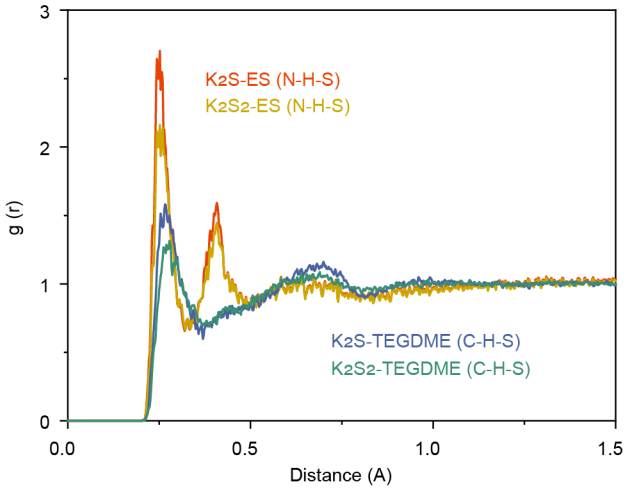

Supplementary Fig. 4. Calculated radial distribution function of molecular dynamics (MD) simulations of K_2S and K_2S_2 in CPL/Acetamide Eutectic Solvent (ES) and TEGDME. The larger peak height in ES indicates stronger bonding between S^{2-}/ S_2^{2-} and ES.

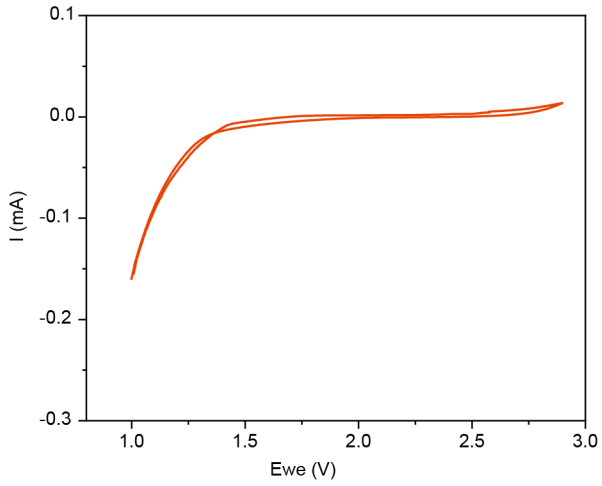

Supplementary Fig. 5. Cyclic voltammetry plot of 0.5 M KTFSI in CPL/acetamide from 1.0 V to 3.0 V, with K-Na alloy as the counter electrode.

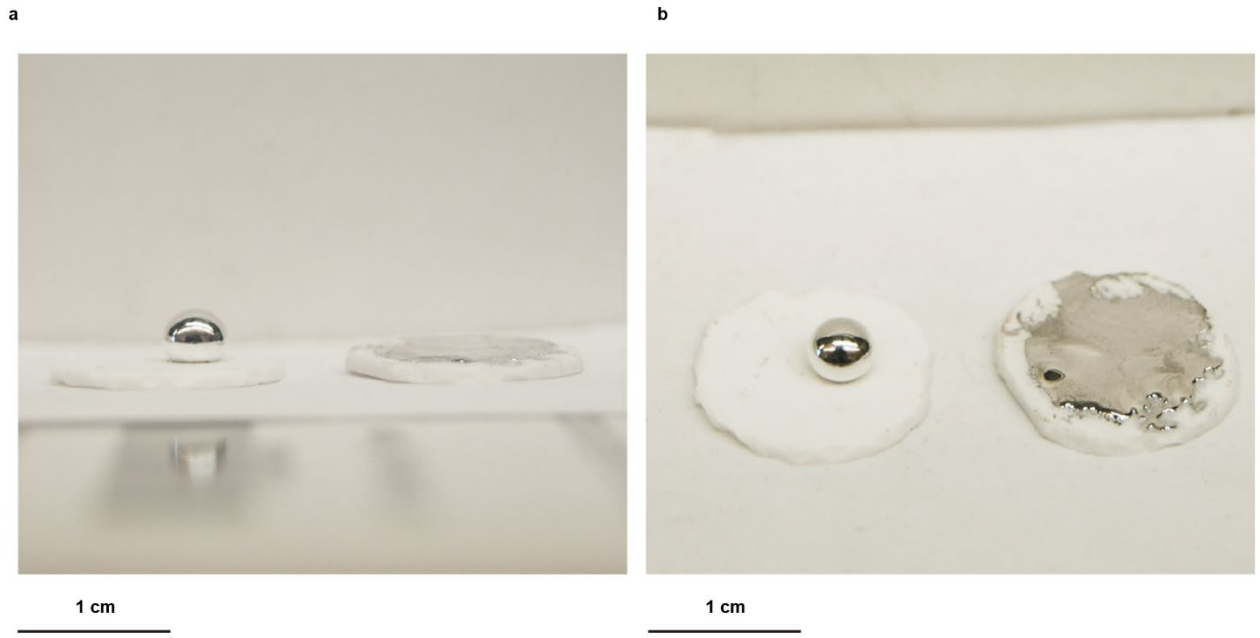

Supplementary Fig. 6. (a) K-Na alloy on a BASE sheet. (b) K-Na alloy with carbon powder on a BASE sheet. The temperatures in both figures are 75 ºC.

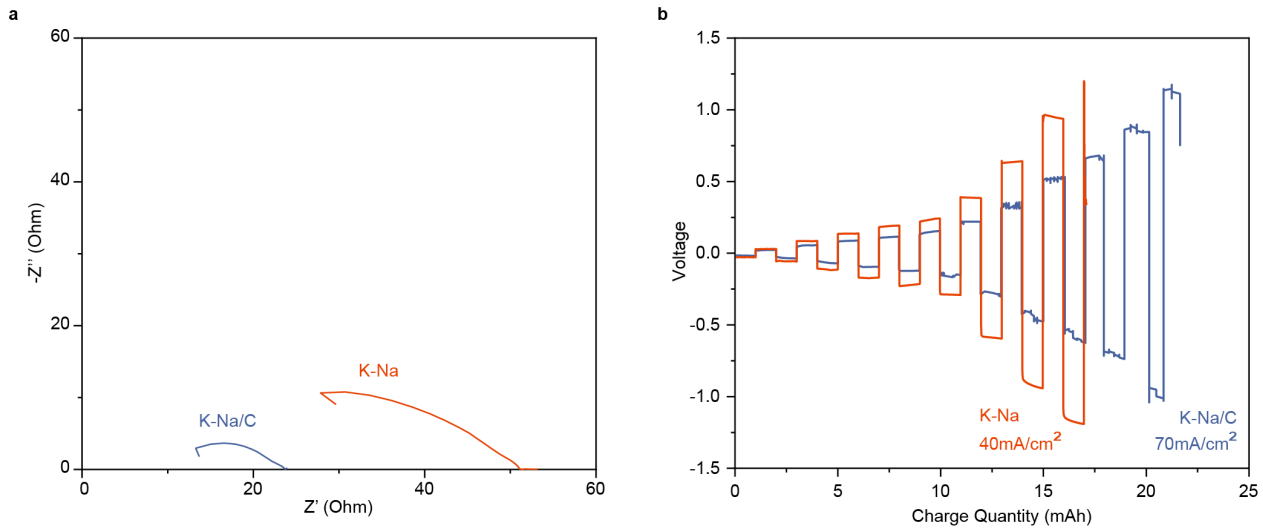

Supplementary Fig. 7. (a) Impedance results of symmetry cell with K-Na/C or K-Na alloy as electrode in both sides. The interfacial impedance of K-Na alloy/BASE is reduced from ~21 ohm without CB to ~7 ohm with CB. As EIS includes charge transfer impedance of two K-Na alloy/BASE interfaces in a symmetric cell, so the impedance of one interface should be the measured value divided by 2. (b) Critical current density tests for symmetry cell with K-Na/C or K-Na alloy as electrode in both sides. The current densities from left to right are 0.5, 1, 2, 3, 4, 5, 6, 7, 8, 9, 10, 15, 20, 25, 30, 35, 40, 45, 50, 60, 70 mA cm^{-2}. The results show that the critical current density of K-Na/C is significantly higher than K-Na alloy.

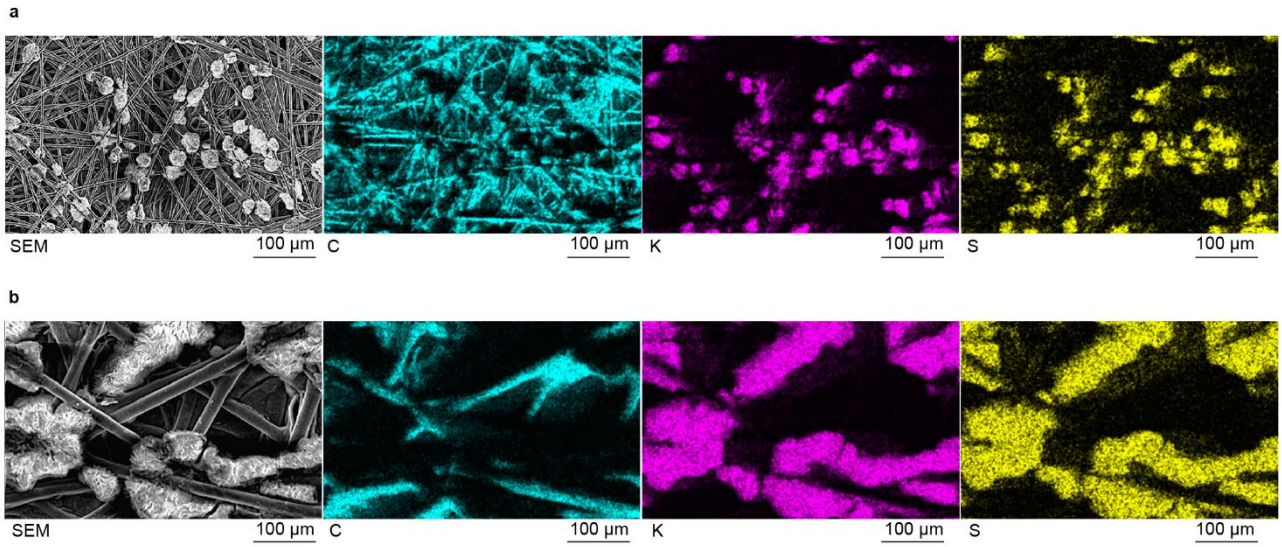

Supplementary Fig. 8. Energy Dispersive Spectroscopy (EDS) mapping for C, K and S element for precipitation in TEGDME catholyte in 100X (a) and 500X (b).

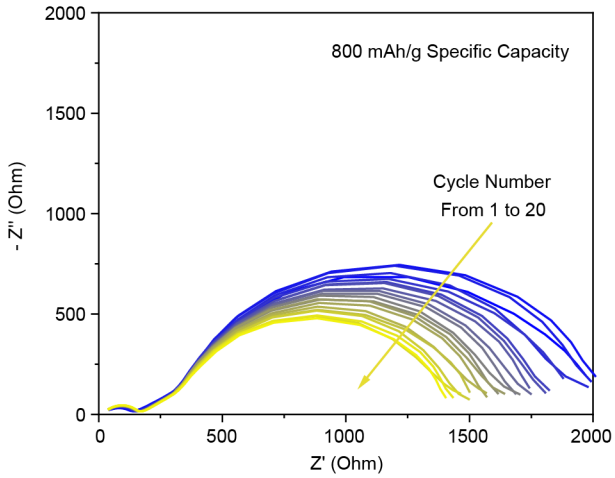

Supplementary Fig. 9. Impedance results in the first 20 cycles of 4M [S] K-Na/S cells running at 75°C. All measurements are done at the same state of discharge (discharge to 800 mAh/g).

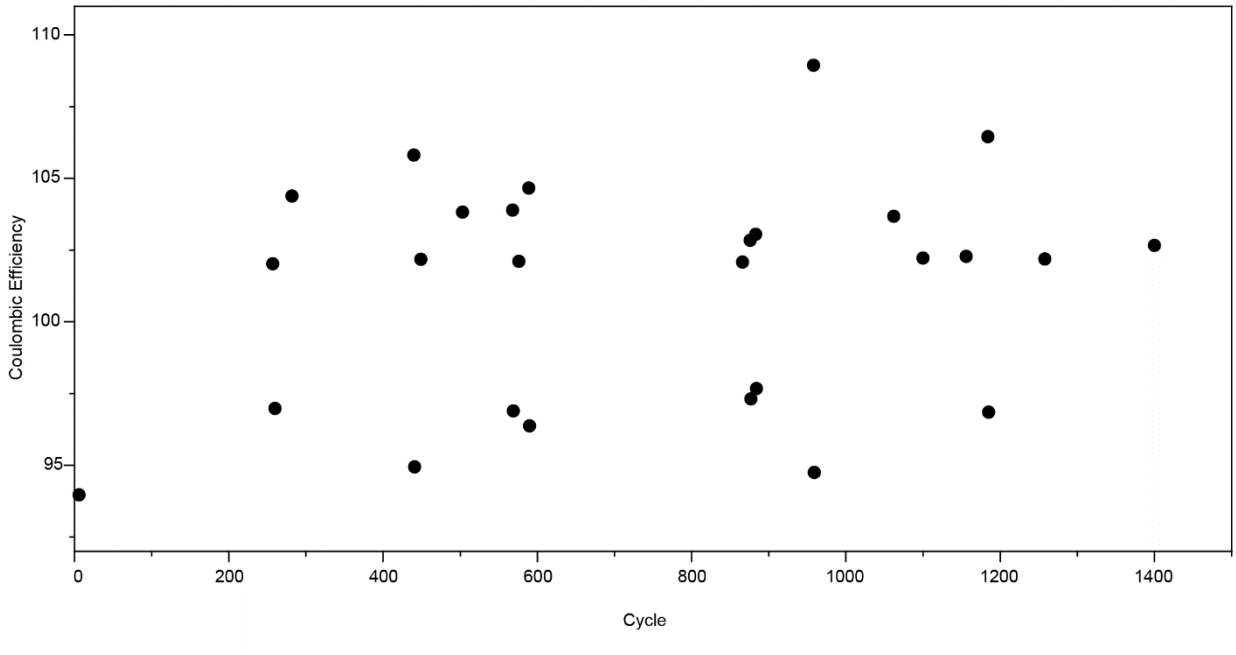

Supplementary Fig. 10. Irregular coulombic efficiency (<98% or >102%) for 4 M CPL/acetamide cells with the current density of 2 mA/cm^2 during 1500 cycle. The frequency of "abnormal" CE (> 102% or <98%) is about once every 50 cycles (roughly 10 days). And typically, a high CE > 102% and a low CE < 98% often occur as a group, so the excessive discharge capacity and the deficient discharge capacity cancel out. As a consequence, the fluctuation is unlikely to come from the system's intrinsic properties, and could come from the external perturbation (e.g., disruptions of connecting wires, sharp temperature change due to opening the oven).

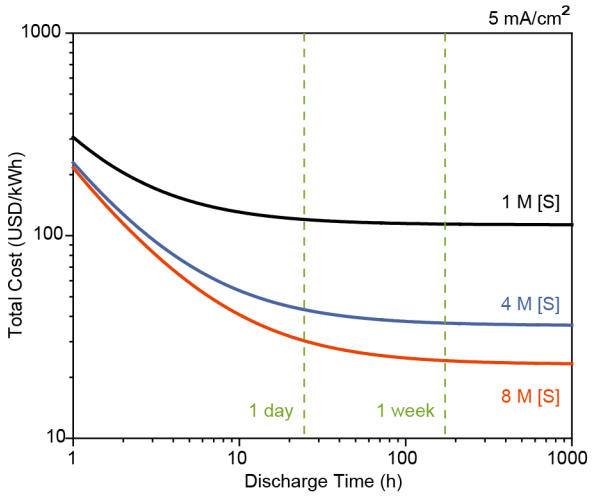

Supplementary Fig. 11. The discharge time dependence of material cost for K-Na/S battery with 1 M [S] /4 M [S] /8 M [S] at 5 mA cm^{-2}. All assumptions are the same as Supplementary Note 7. For 4 M [S], the costs for 1 day discharge and 1 week discharge are \$42 and \$36 /kWh, respectively. For 8 M [S], the costs for 1 day discharge and 1 week discharge are \$29 and \$23 /kWh, respectively.

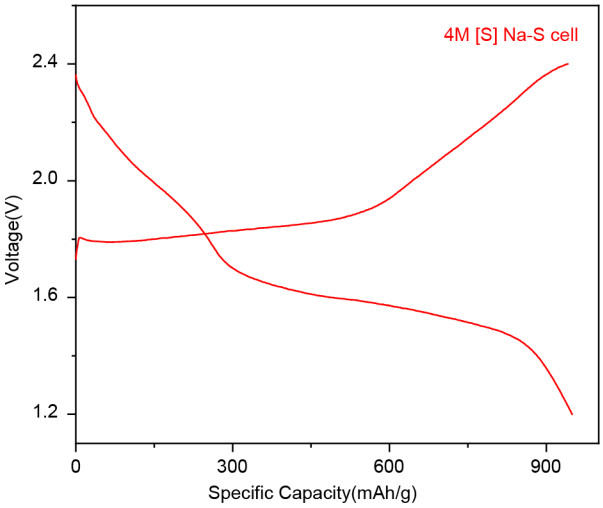

Supplementary Fig. 12. The voltage profile of the first cycling in 4M [S] Na-S cells running at 85 ºC. 10% molar ratio of Cs metal is used as an additive to improve wetting towards Na-BASE sheet.

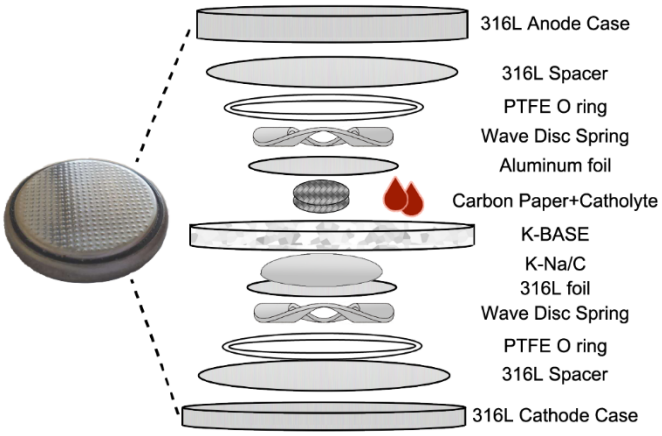

Supplementary Fig. 13. Schematic of K-Na/S coin cell configuration.

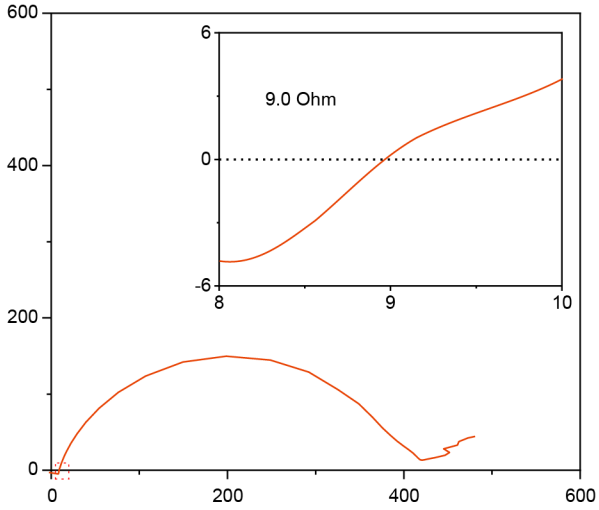

Supplementary Fig. 14. Impedance measurement for $Na_2S_{2.8}$ in CPL/acetamide catholyte in a cell with two Cu current collectors for conductivity measurements.

Supplementary References

1 Kim, H. *et al.* Enhanced reversible capacity of sulfurized polyacrylonitrile cathode for room-temperature Na/S batteries by electrochemical activation. *Chem Eng J* **426** (2021). https://doi.org/10.1016/j.cej.2021.130787

2 Zhang, S. *et al.* Mo2N–W2N Heterostructures Embedded in Spherical Carbon Superstructure as Highly Efficient Polysulfide Electrocatalysts for Stable Room-Temperature Na–S Batteries. *Advanced Materials* **33**, 2103846 (2021). https://doi.org/10.1002/adma.202103846

3 Yan, Z. *et al.* A High-Kinetics Sulfur Cathode with a Highly Efficient Mechanism for Superior Room-Temperature Na–S Batteries. *Advanced Materials* **32**, 1906700 (2020). https://doi.org/10.1002/adma.201906700

4 Guo, Q. B. *et al.* Ultrastable Sodium-Sulfur Batteries without Polysulfides Formation Using Slit Ultramicropore Carbon Carrier. *Advanced Science* **7** (2020). https://doi.org/10.1002/advs.201903246

5 Jiang, Y. *et al.* Single-Atom Vanadium Catalyst Boosting Reaction Kinetics of Polysulfides in Na–S Batteries. *Advanced Materials* **35**, 2208873 (2023). https://doi.org/10.1002/adma.202208873

6 Yang, H. *et al.* Architecting Freestanding Sulfur Cathodes for Superior Room-Temperature Na–S Batteries. *Advanced Functional Materials* **31**, 2102280 (2021). https://doi.org/10.1002/adfm.202102280

7 Wang, Y. *et al.* Tunable Electrocatalytic Behavior of Sodiated MoS2 Active Sites toward Efficient Sulfur Redox Reactions in Room-Temperature Na–S Batteries. *Advanced Materials* **33**, 2100229 (2021). https://doi.org/10.1002/adma.202100229

8 Xiong, P. *et al.* Room-Temperature Potassium–Sulfur Batteries Enabled by Microporous Carbon Stabilized Small-Molecule Sulfur Cathodes. *ACS Nano* **13**, 2536-2543 (2019). https://doi.org/10.1021/acsnano.8b09503

9 Ge, X. *et al.* Metal–Organic Framework-Derived Nitrogen-Doped Cobalt Nanocluster Inlaid Porous Carbon as High-Efficiency Catalyst for Advanced Potassium–Sulfur Batteries. *ACS Nano* **14**, 16022-16035 (2020). https://doi.org/10.1021/acsnano.0c07658

10 Lai, N. C., Cong, G. T. & Lu, Y. C. A high-energy potassium-sulfur battery enabled by facile and effective imidazole-solvated copper catalysts. *J Mater Chem A* **7**, 20584-20589 (2019). https://doi.org/10.1039/c9ta06906b

11 Wang, L., Bao, J. Z., Liu, Q. & Sun, C. F. Concentrated electrolytes unlock the full energy potential of potassium-sulfur battery chemistry. *Energy Storage Mater* **18**, 470-475 (2019). https://doi.org/10.1016/j.ensm.2018.10.004

12 Lu, X. *et al.* Advanced intermediate-temperature Na–S battery. *Energy & Environmental Science* **6**, 299-306 (2013). https://doi.org/10.1039/C2EE23606K

13 Lu, X. *et al.* Liquid-metal electrode to enable ultra-low temperature sodium–beta alumina batteries for renewable energy storage. *Nature Communications* **5**, 4578 (2014). https://doi.org/10.1038/ncomms5578

14 Tai, Z. *et al.* Novel Quasi-Liquid K-Na Alloy as a Promising Dendrite-Free Anode for Rechargeable Potassium Metal Batteries. *Advanced Science* **8**, 2101866 (2021). https://doi.org/10.1002/advs.202101866

15 Lu, X. C., Bowden, M. E., Sprenkle, V. L. & Liu, J. A Low Cost, High Energy Density, and Long Cycle Life Potassium-Sulfur Battery for Grid-Scale Energy Storage. *Advanced Materials* **27**, 5915-5922 (2015). https://doi.org/10.1002/adma.201502343

16 Xin, S. *et al.* Smaller Sulfur Molecules Promise Better Lithium-Sulfur Batteries. *Journal of the American Chemical Society* **134**, 18510-18513 (2012). https://doi.org/10.1021/ja308170k

17 Guo, J. C., Xu, Y. H. & Wang, C. S. Sulfur-Impregnated Disordered Carbon Nanotubes Cathode for Lithium-Sulfur Batteries. *Nano Lett* **11**, 4288-4294 (2011). https://doi.org/10.1021/nl202297p

18 β-alumina (NaAl11O17) Crystal Structure: Datasheet from "PAULING FILE Multinaries Edition – 2022" in SpringerMaterials (https://materials.springer.com/isp/crystallographic/docs/sd_1410950) (Springer-Verlag Berlin Heidelberg & Material Phases Data System (MPDS), Switzerland & National Institute for Materials Science (NIMS), Japan).

19 Zhang, Y., Squire, H., Gurkan, B. & Maginn, E. J. Refined classical force field for choline chloride and ethylene glycol mixtures over wide composition range. *J. Chem. Eng. Data* **67**, 1864-1871 (2022).

20 Darden, T., York, D. & Pedersen, L. Particle mesh Ewald: An N· log (N) method for Ewald sums in large systems. *The Journal of chemical physics* **98**, 10089-10092 (1993).

21 Berendsen, H. J., van der Spoel, D. & van Drunen, R. GROMACS: A message-passing parallel molecular dynamics implementation. *Comput. Phys. Commun.* **91**, 43-56 (1995).

22 Shirts, M. R. & Chodera, J. D. Statistically optimal analysis of samples from multiple equilibrium states. *The Journal of chemical physics* **129**, 124105 (2008).

23 Straatsma, T. & McCammon, J. Computational alchemy. *Annu. Rev. Phys. Chem.* **43**, 407-435 (1992).

24 Lu, X. C. *et al.* Liquid-metal electrode to enable ultra-low temperature sodium-beta alumina batteries for renewable energy storage. *Nat. Commun.* **5**, 8 (2014). https://doi.org/10.1038/ncomms5578

25 Zhang, L. Y. *et al.* Non-Newtonian Fluid State K-Na Alloy for a Stretchable Energy Storage Device. *Small Methods* **3**, 9 (2019). https://doi.org/10.1002/smtd.201900383

26 Vapor Pressure of Pure Substances - Inorganic Compounds. *Ind Eng Chem* **39**, 540-550 (1947).

27 Chaudhari, S. K., Patil, K. R., Allepus, J. & Coronas, A. Measurement of the Vapor-Pressure of 2,2,2-Trifluoroethanol and Tetraethylene Glycol Dimethyl Ether by Static Method. *Fluid Phase Equilibr* **108**, 159-165 (1995). https://doi.org/10.1016/0378-3812(95)02683-6

28 Liu, B. Y., Zhao, J. J. & Wei, F. X. Characterization of caprolactam based eutectic ionic liquids and their application in SO2 absorption. *J Mol Liq* **180**, 19-25 (2013). https://doi.org/10.1016/j.molliq.2012.12.024